Journal of Physics: Conference Series

Improved fatigue life of floating offshore wind turbine towers with tuned mass damper inerters (TMDIs)

To cite this article: J McAuliffe *et al* 2024 *J. Phys.: Conf. Ser.* **2647** 032007

Journal of Physics: Conference Series **2647** (2024) 032007 doi:10.1088/1742-6596/2647/3/032007

Improved fatigue life of floating offshore wind turbine towers with tuned mass damper inerters (TMDIs)

J McAuliffe, S Baisthakur, B Broderick and B Fitzgerald

Department of Civil, Structural and Environmental Engineering, School of Engineering, Trinity College Dublin, Ireland

E-mail: breiffni.fitzgerald@tcd.ie, jmcaulif@tcd.ie, baisthas@tcd.ie, brian.broderick@tcd.ie

Abstract. Floating offshore wind turbines (FOWTs) are the largest rotating structures on earth. FOWTs are very flexible and dynamically sensitive, they are also installed in very harsh environments and exposed to stochastic environmental loading from wind and ocean waves. In recent years dampers have been installed in the towers of offshore wind turbines to mitigate vibrations. In this paper, structural dynamic models are used to demonstrate improvements in the fatigue life of FOWT towers when they are equipped with a new type of damper - the tuned mass damper inerter (TMDI). A multi-body dynamic approach is used to model the wind turbine and the TMDI installed in the tower. The model is subjected to stochastically generated wind and wave loads of varying magnitudes to develop wind-induced probabilistic demand models for towers of FOWTs under model and load uncertainties. Numerical simulations are carried out to determine the improvements in fatigue life of FOWT towers that can be achieved by installing TMDIs in comparison to traditional tuned mass dampers (TMDs). The results show that the TMDI outperforms the classical TMD when considering fatigue life.

1. Introduction

Over one-fourth of the cost of producing energy via wind turbines is derived from the operation and maintenance costs [1], by decreasing mechanisms of failure, the price of wind energy production can be further reduced. As modern wind turbines attempt to capture increased amounts of energy, turbines have increased dramatically in size with many beginning to be located in offshore locations. Today's modern multi-megawatt wind turbines are the largest rotating structures in the world [2], with hub heights of over 150 meters and rotor diameters exceeding 240 meters. Modern offshore wind turbines are subject to harsh environmental loading being exposed to highly fluctuating wind speeds, volatile sea states, and a highly corrosive marine environment. In addition to this, the operation of wind turbines induces additional cyclic self-loads to components. Over a lifetime of 20 years, wind turbines experience more than 10^8 load cycles [3] while experiencing a range of weather conditions including variations in temperature, humidity, precipitation, and sunlight. As a consequence of these factors, wind turbines are now experiencing larger and increasingly fluctuating loads, thus the phenomenon of fatigue as a failure mechanism in modern wind turbines is increasing. By implementing design strategies such as the introduction of auxiliary damping devices the fatigue loads experienced by wind turbines may be reduced and as a result, reduce the cost incurred by operation and maintenance.

Fatigue has been studied for many years and for many different applications with early work

Journal of Physics: Conference Series **2647** (2024) 032007 doi:10.1088/1742-6596/2647/3/032007

by Wöhler [4] proposing a simplistic approach to characterise fatigue, the so called S-N curve. This is a plot of Stress (S) vs Number of cycles to failure (N), also named the Wöhler curve. Miner proposed a method of calculating the existing fatigue damage of a component based on the concept that damage can be broken down into increments of damage (partial damage) which can be summed together to achieve the total damage. Palmgren-Miner's rule can be expressed by the simplistic formula:

$$\mathbf{D} = \sum \frac{\mathbf{n_i}}{\mathbf{N_i}} \tag{1}$$

Where D is the total damage sustained, n_i are the number of applied cycles at a given stress and N_i is the number of cycles to failure at a given stress range based on S-N curves. When the damage sustained equals unity the material fails.

Most structures do not experience constant amplitude loading. As a result, a method is required to convert complex time histories into constant amplitude events to allow them to be used with S-N curves and Palmgren-Miner's Rule. Endo proposed the 'Rainflow counting' method to address this problem. The key steps involved in Rainflow counting method can be found in [5]. Since the late 60s, the method has been used extensively to calculate fatigue in structures such as wind turbines [6, 7, 8, 9] and many adaptations of the method have been implemented [10, 11].

As discussed, large tower and blade deflections are leading to increased fatigue damage in wind turbines as these structures increase in size. In an attempt to reduce these responses, tuned mass dampers (TMD) have been used by designers. A TMD is a control device that is used in flexible structures to reduce vibrations caused by dynamic loading. The reduction of induced loads and deflections via the installation of TMDs in wind turbine towers and blades has been investigated in depth [12, 13, 14, 15, 16]. Despite encouraging results, the large mass ratios required and lack of adaptability make TMDs a substandard vibration controller for offshore wind turbines [17]. Many studies have proposed alternative dampers and various adaptations of the TMD to address its shortcomings such as active TMDs [18, 19, 20], semi-active TMDs [21] and tuned liquid column dampers [22]. A novel damping device, which has recently been investigated for potential use in wind turbines is the Tuned Mass Damper Inerter (TMDI). The TMDI operates in a similar manner to the traditional TMD with the addition of an inerter to the system. The inerter component is added in parallel to the existing spring and damper. The inerter is a flywheel that converts linear motion into high-speed rotational motion and as a result, amplifies the effective mass of the TMD. This amplification provides increased performance of the device allowing for increased reductions in load and displacement without the necessity of increasing the mass ratio of the damping device.

Since their introduction in 2002 by Smith [23], a number of studies have been carried out investigating and optimising the damping capabilities of TMDIs in modern wind turbines. Hu et al [24] successfully implemented a H_2 optimisation method to select the optimum parameters of a inerter-based dynamic vibration absorber (IDVA) in order to reduce the loads experienced by wind turbines under a range of rotational frequencies.

Zhang et al [25] reduced the tower top displacements, base shear, and bending moments of a wind turbine subject to seismic excitations by installing tuned parallel inerter mass systems (TPIMS). Sarkar et al [26] reduced both tower displacements and damping device stroke by introducing an ineter to a traditional TMD in a spar-type offshore wind turbine. Sarkar and Fitzgerald [27] installed a tuned mass damper fluid inerter (TMDFI) in the nacelle of NREL's 5 MW spar-type floating offshore wind turbine. The TMDFI greatly outperformed traditional TMDs in reducing the vibration response of the turbine while also offering the added advantage of low maintenance costs and reduced downtime due to its simplistic design.

The above literature and previous work by the authors have shown the potential for reductions

Journal of Physics: Conference Series **2647** (2024) 032007 doi:10.1088/1742-6596/2647/3/032007

in displacements and induced loading that can be achieved as a result of installing a TMDI in the nacelles of FOWT towers [26, 27]. The advantages of TMDIs over traditional TMDs are clear with additional reductions in both mass ratios and device stroke displacements easily achieved. However, in the above literature, little work has been carried out with regard to the potential use of TMDIs for the reduction of fatigue damage loads. In this paper, we address this gap in knowledge by assessing the tower fatigue damage loads of NREL's 5 MW wind turbine supported by OC3 Hywind spar-buoy platform when a TMDI is installed in the nacelle.

Based on the literature presented above, this paper:

- Produces stress time histories for the turbine tower using a 22-degree-of-freedom numerical simulation model which has been verified against NRELs FAST software.
- Calculates tower fatigue damage equivalent loads using MLife software, which is designed based on Palmgren Miners rule and rainflow counting.
- Demonstrates reductions in FOWT tower fatigue damage loads when tuned mass damper inerters (TMDIs) are installed, paying particular attention to the less damped side-to-side direction where the dampers are most effective.
- Examines the effect of wind speed on the effectiveness of tuned mass damper inerters (TMDIs) when installed in the nacelle of FOWT with active pitch control.

The results indicate that the TMDI reduces the fatigue damage loads for all examined met-ocean conditions and thus it improves the fatigue life of the FOWT. The TMDI significantly reduces the wind-induced fatigue loads experienced by the FOWT towers when operating in region 2 and at wind speeds above the rate wind speed of the turbine. For an equal damper mass, a TMDI is more effective in reducing fatigue loads in comparison with traditional dampers.

2. 5-MW FOWT tower coupled with TMDI - Numerical Simulations

Stress time histories at the turbines tower base were obtained by performing numerical simulations carried out using a nonlinear aeroelastic multi-body dynamic model of NREL's 5 MW wind turbine defined in [28], with the OC3 Hywind spar-buoy platform defined in [29]. The properties of this turbine can be seen in Table 1. The model is fully coupled with 22 degrees of freedom which was developed using Kane's Dynamics [30].

Kane's equations of motion for a simple holonomic multi-body system can be expressed as:

$$F_k + F_k^* = 0 \qquad \text{for } k = 1, 2, ... \ N \tag{2}$$

where N is the total number of degrees of freedom of the system, in the case of the FOWT there are twenty-two degrees of freedom stemming from the platform, tower, yaw bearing, nacelle, hub, blades and generator.

The *generalized active force,* F_k for the k^{th} degree of freedom can be found for a set of M rigid bodies characterized by reference frame N_i and center of mass point X_i by:

$$F_k = \sum_{i=1}^{M} \left[{}^E\mathbf{v}_k^{X_i} \cdot \mathbf{F}^{X_i} + {}^E\omega_k^{N_i} \cdot \mathbf{M}^{N_i} \right] \tag{3}$$

where $\mathbf{F}^{X_i}$ is force vector acting on the center of mass of point X_i and $\mathbf{M}^{N_i}$ is the moment vector acting on the N_i rigid body. ${}^E\mathbf{v}_k^{X_i}$ and ${}^E\omega_k^{N_i}$ are the partial linear and partial angular velocity of the point X_i and rigid body N_i respectively associated with the k^{th} degree of freedom in the inertial (E) reference frame. The *generalized inertia force* for k^{th} degree of freedom is given as:

$$F_k^* = -\sum_{i=1}^{M} \left[{}^E\mathbf{v}_k^{X_i} \cdot \left(m^{N_i}\, {}^E\mathbf{a}^{X_i} \right) + {}^E\omega_k^{N_i} \cdot {}^E\dot{\mathbf{H}}^{N_i} \right] \tag{4}$$

where it is assumed that for each rigid body N_i, the inertia forces are applied at the centre of the mass point X_i. ${}^{E}\dot{\mathbf{H}}^{N_i}$ is the time derivative of the angular momentum of the rigid body N_i about its center of mass X_i in the inertial frame [30].

The hydrodynamic loads in the model are calculated using Morrison's equation while aerodynamic loads are calculated using blade-element momentum theory. Mooring cable loads are calculated using MoorDyn software [31]. Additional forces applied to the model include gravitational forces, generator torque forces and forces in the high-speed shaft brake. The gearbox friction forces have not been included in this model. Constraints relationships between rigid bodies are enforced using yaw springs and damper forces while flexible members' internal forces are calculated based on their elasticity and damping. This model has been developed and benchmarked previously by the authors against the National Renewable Energy Laboratory's (NREL) fully coupled nonlinear simulation code, OpenFAST [32], for full information regarding the modeling see [33, 34, 26].

Table 1. Properties of NREL 5-MW OC3-Hywind spar-type FOWT [28]

NREL 5-MW OC3-Hywind spar-type FOWT properties		
Basic description	Max rated power	5-MW
	Rotor orientation, configuration	Upwind, 3 blades
	Rotor diameter	126m
	Hub height	90m
	Cut-in, rated, cut-out wind speed	3m/s, 11.4m/s, 25m/s
	Cut-in, rated rotor speed	6.9 rpm, 12.1 rpm
Tower	1^{st} Fore-Aft mode natural frequency	0.324 Hz
	1^{st} Side-to-Side mode natural frequency	0.312 Hz
	Structural-damping ratio (all modes)	1%
	Material	S355 Steel
	Yeild Strength	355 MPa
	Wöhler exponent	4

The TMD and TMDI are installed at the top of the FOWT tower as shown in Figure 1. The introduction of the damping device introduces a 23rd degree of freedom to the model which is easily incorporated into the model due to the simplistic nature of the Kanes Dynamics Equation. The key to introducing the damping devices into the dynamic equations is defining the kinematic description of the dampers including the position, velocity and acceleration vectors at all important points on the FOWT. The position vector at the top of the FOWT tower can be simply expressed as:

$$r^{OD} = \begin{cases} q_D\hat{\mathbf{b}}_\mathbf{3} & \text{coupled to side-to-side direction} \\ q_D\hat{\mathbf{b}}_\mathbf{1} & \text{coupled to fore-aft direction} \end{cases} \tag{5}$$

where D denotes the centre of mass of the damper, q_D is the displacement of the damper from its neutral position and $\hat{b}$ is the coordinate system at the top of the tower.

The forces from the spring, damper and inerter are incorporated in equation (3) contributing to the generalized active forces while the mass of the damping device is incorporated into equation (4) contributing to the generalized inertia forces. Using the time derivatives of the

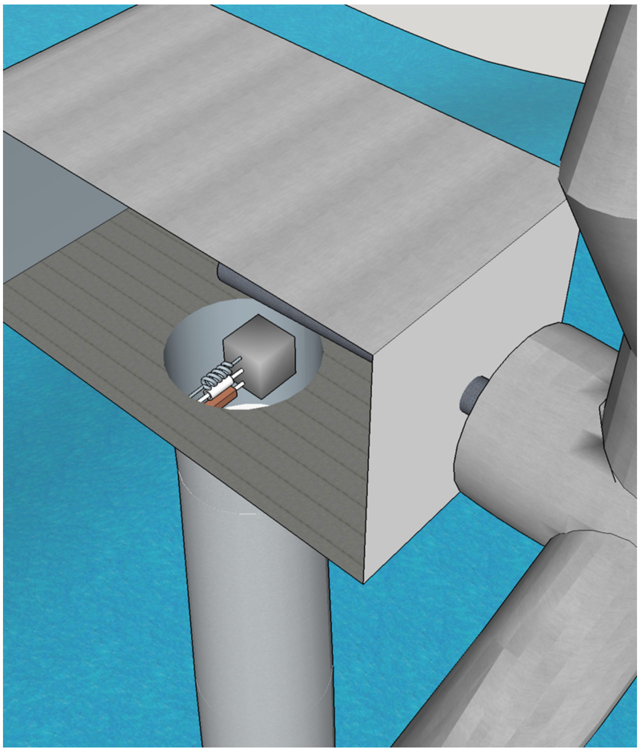

Figure 1. Floating offshore wind turbine with TMDI

generalized coordinates of the system, both partial linear and angular velocities of all important points and rigid bodies can be defined and used to write the non-linear time-domain equations of motion. These can be written in their general form as:

$$\mathbf{M}(\mathbf{q}, \mathbf{u}, t)\ddot{\mathbf{q}} = -\mathbf{f}(\dot{\mathbf{q}}, \mathbf{q}, \mathbf{u}, t) \quad (6)$$

where, $\mathbf{M}$ is the inertial mass matrix that is a non-linear function of the set of degrees of freedom $\mathbf{q}$, control input $\mathbf{u}$, and time t. The force vector $\mathbf{f}$ depends non-linearly on the degrees of freedom, the time derivative of the degrees of freedom, control input and time.

The numerical simulations were performed via MATLAB ® [35] utilising the Runga-Kutta 'ODE 4' method to solve the non-linear numerical system obtaining stress time histories at the tower base for three separate scenarios: no active dampers, TMD active, and TMDI active. The TMD optimum parameters were calculated utilising equation 7, given by Luft [36].

$$\xi_{TMD} = \frac{\sqrt{\mu_{TMD}}}{2} \quad (7)$$

For the TMDI, closed-form expressions for the optimum tuning and damping parameters of TMDIs installed in FOWT towers are implemented which were developed by Sarkar [26]. For both the TMD and TMDI a mass ratio of 1% of the tower mass was applied. An inertance of $\beta = 0.4$ was selected based on Sarkar et al's [26] finding that vibration control becomes saturated at inerter ratios greater than 0.4.

2.1. Numerical Simulations - Design of Experiment

Three different met-ocean scenarios are considered for this research, calm, mild, and rough, the details of which can be found in Table 2. For each of the met-ocean conditions 40 wind speeds are considered which were selected using Latin Hypercube Sampling (LHS) between the values of 3 m/s and 25 m/s, the cut-in and cut-out wind speeds of the 5-MW FOWT respectively [28]. A turbulence intensity of 10% for each of the wind speeds was selected. In accordance with IEC 61400-3-1 [37], for each environmental condition, six ten-minute simulations were carried out. As a result, six wind files with six random seeds were paired with a corresponding wave file also having been generated with a random seed. The wind files were generated using TurbSim [38] a software package distributed by NREL. Linear Airy wave theory is used to generate the wave files used in the model with the stochastic sea modeled using the Pierson-Moskowitz spectrum [39]. Simulations were carried out on each pair of files with no damper active, TMD active, and TMDI active. This resulted in a total of 2160 (3 damper states × 3 met-ocean conditions × 40 wind speeds × 6 seeds) simulations to be carried out. Each of the simulations had a duration of 675 seconds with the initial 75 seconds removed in order to eliminate the effect of the initial transient phase.

Table 2. Met-ocean conditions

Load Case	*Wave Conditions*	*Significant Height, Hs(m)*	*Peak Period, Tp (s)*
LC1	Calm Sea	0.75	6
LC2	Moderate Sea	2.25	6.25
LC3	Rough Sea	6	8

2.2. MLife - fatigue damage equivalent load calculations

NREL's software pack MLife [40] was used to calculate the fatigue Damage Equivalent Loads (DEL) using the results of the numerical simulations. The DELs were calculated based on a zero fixed mean. A Weibull probability distribution was implemented for wind speeds with a shape factor of 2 and a scale factor of 10. For the DELs an ultimate load (LUlt) of 355 Mpa was used while an equivalent frequency of 1 hz was utilised. In order to investigate the effectiveness of the dampers at the various wind speeds, the short-term DEL was investigated at each individual wind speed. For each wind speed, the six-time histories, which were obtained from the numerical simulations for a given set of met-ocean conditions were grouped together using MLifes aggregate function to find the short-term DEL for a given wind speed. This process was repeated for each of the damping states. The DEL at each wind speed was compared against the baseline (original) turbine as a percentage (%) reduction in short-term DEL. The lifetime fatigue DEL for each of the met-ocean conditions was calculated by inputting all six time history files for all 40 wind speeds. The DEL for a 20-year span was calculated and again compared against the baseline condition as a percentage (%) reduction in lifetime DEL.

3. Results and discussion

The effectiveness of the controllers implemented are investigated via both short-term and long-term DELs. The long-term DELs are presented in table 3. In the table, the long-term DELs with an active TMDI and an active TMD are compared with DEL of the wind turbine with no active dampers. Additionally, the DELs with an active TMD is compared with DELs with an active TMDI in order to highlight reductions in long-term DELs provided by adding the inerter to the system. The short-term fatigue is examined in figures 2 and 3. For short-term DELs each wind speed is examined individually. Again the baseline condition is compared with the active TMD and TMDI.

Journal of Physics: Conference Series **2647** (2024) 032007 doi:10.1088/1742-6596/2647/3/032007

Table 3. Lifetime DEL Results: Percentage reduction of DELs (Uncontrolled model vs controlled)

$Met - Ocean\ Condition$	$Damper\ Direction$	$TMD(\%)$	$TMDI(\%)$	$TMD\ vs\ TMDI(\%)$
LC1	FA	−2.3	−10.4	−8.3
LC2	FA	−1.8	−7.3	−5.6
LC3	FA	−0.46	−0.46	0.0
LC1	SS	−29.7	−48.6	−26.8
LC2	SS	−34.3	−54.8	−31.2
LC3	SS	−41.4	−63.1	−37.2

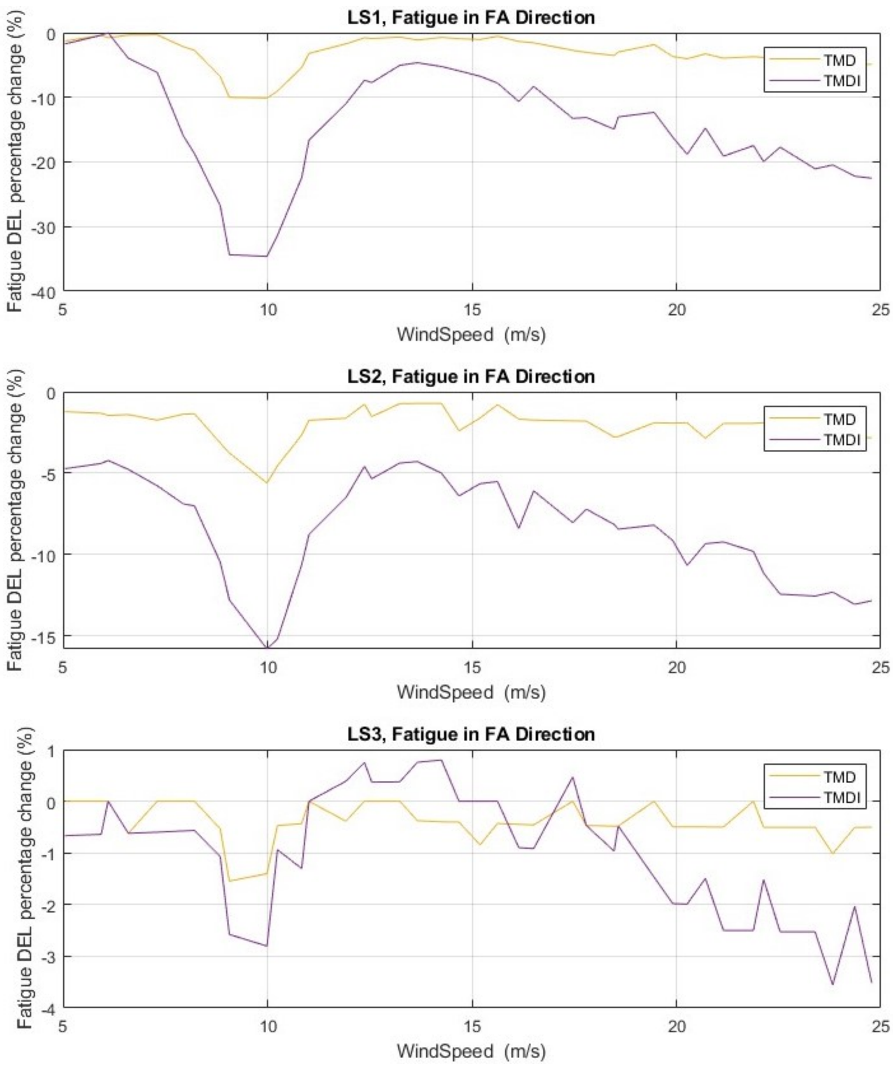

Figure 2. Fatigue DEL (%) reduction in FA direction with dampers active in FA Direction

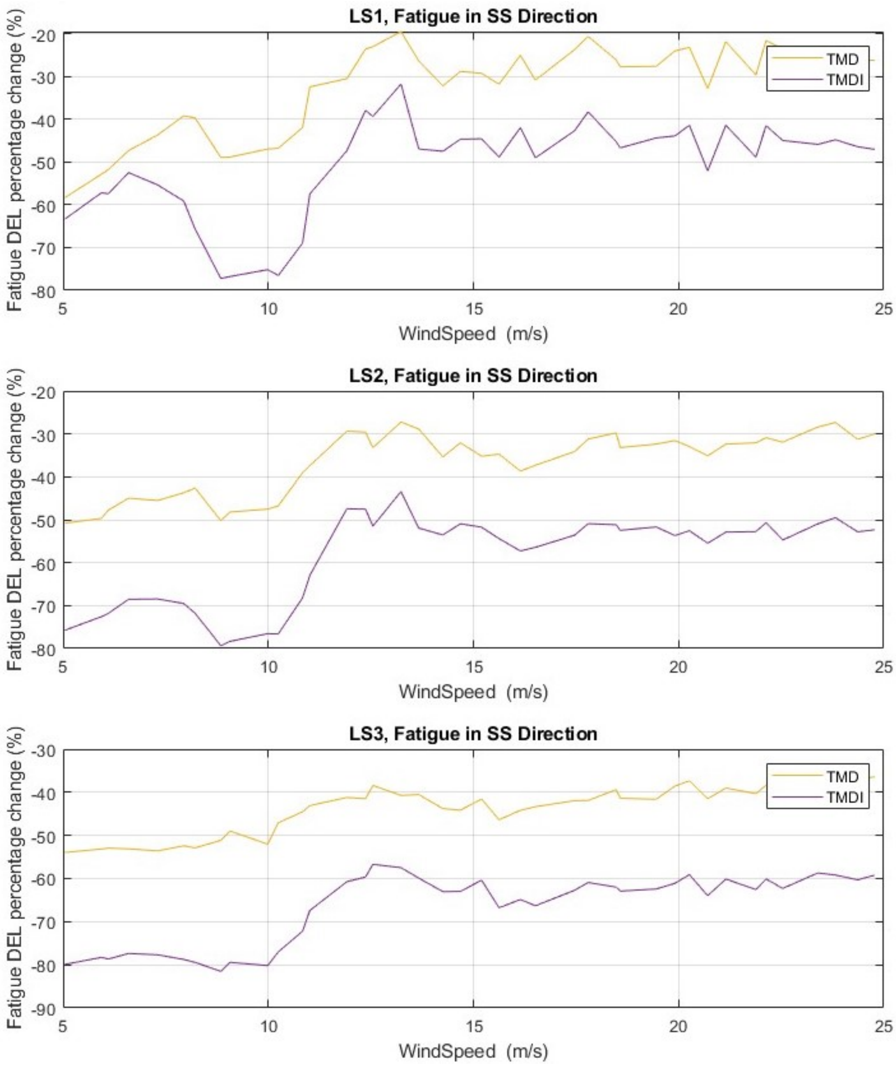

Figure 3. Fatigue DEL (%) reduction in SS direction with dampers active in SS Direction

The results in table 3 demonstrate the reduction in long-term fatigue loads that can be achieved by the introduction of a TMD or TMDI. From the table, it is clear that the dampers are much more effective in the side-to-side direction with the TMDI providing fatigue reductions of over 63% in comparison to just over 10% in the fore-aft direction. This large difference in efficacy arises due to the pre-existing damping in the fore-aft direction provided by the turbine blades. This hence reduces the effectiveness and thus requirement for a damping system in the fore-aft direction. However, in the undamped direction, the full potential of the TMD and TMDI are realised producing large reductions in fatigue damage. The TMD is seen in table 3 to decrease the fatigue load experienced by the turbine tower across all met-ocean conditions. The TMDI provides much larger fatigue reductions than the TMD in all cases with the exception of LC3 in the FA direction, stemming from the pre-existing damping in this direction. For LC3 in the FA directions neither damper provides significant damping. LC3 represents a rough sea state with relatively large tower displacements. Due to the existing damping provided by the turbine blades in the fore-aft direction under large displacements the TMD and TMDI are not effective. However, under the same rough sea state conditions the TMD and TMDI are extremely effective in the side-to-side direction where little pre-existing damping exists.

Figures 2 and 3 illustrate the wind speed ranges where the dampers are most effective. In the fore-aft direction, two patterns can clearly be identified from the results. In region 2 where the turbine is operating between its cut-in wind speed (3m/s) and its rated wind speed (11.4m/s), the dampers have little effect at lower wind speeds, however, as wind speeds increase and approach the rated wind speed their effectiveness improves significantly. The effectiveness of the dampers drops off as the pitch controller is activated above 11.4m/s with the feathering of the blades used to reduce loads experienced by the turbine. As wind speeds increase beyond 11.4m/s, there is once again an increase in the effectiveness of the dampers as loads and displacements begin to increase. The same patterns can be observed for LC3 in the fore-aft direction however due to the rough sea state discussed above the patterns are less obvious. A similar pattern is observed for all three met-ocean conditions in the side-side direction. However, the reductions in the side-to-side direction are much more significant with short-term DELs reductions of over 80% observed. The fatigue damage reductions in the side-to-side direction are much less dependent on the region of operation as feathering of the blades does not heavily influence the side-to-side loads however there is still a drop off in DEL reductions at 11.4m/s which begins to increase again as wind speed increases past the cut in wind speed.

4. Conclusion

This research investigated the influence of placing a TMDI in the nacelle of a wind turbine. The results conclude that the TMDI will reduce fatigue damage in both the fore-aft and side-to-side directions. The TMDI however is much more effective in the side-to-side direction where damping due to the blades is low. The introduction of the inerter to the TMD system greatly increases the damping device's ability to reduce both short term and long-term fatigue loads experienced by the turbine tower. The TMDI was found to be most effective when pitch control is not active, thus at wind speeds below the rated wind speed. The TMDI begins to become increasingly more effective as wind speeds increase beyond the rated wind speed toward the cut-out wind speed. Reductions of over 63% in long-term fatigue damage have been observed in the side-to-side direction with the addition of the TMDI while reductions of over 80% in short-term fatigue damage have been observed for selected wind speeds.

5. Acknowledgements

The Funding for this research was provided by the Sustainable Energy Authority of Ireland (SEAI) under the WindLEDeRR project, grant number RDD 601.

The authors are thankful for the support received.

6. References

[1] Liao D, Zhu S P, Correia J A, Jesus A M, Veljkovic M and Berto F 2022 *Renewable Energy*
[2] Van Kuik G, Peinke J, Nijssen R, Lekou D, Mann J, Sørensen J N, Ferreira C, van Wingerden J W, Schlipf D, Gebraad P *et al.* 2016 *Wind energy science* **1** 1–39
[3] Kensche C W 2006 *International journal of fatigue* **28** 1363–1374
[4] Wöhler A 1870 *Über die festigkeitsversuche mit eisen und stahl* (Ernst & Korn)
[5] Downing S D and Socie D 1982 *International journal of fatigue* **4** 31–40
[6] Dong W, Moan T and Gao Z 2011 *Engineering Structures* **33** 2002–2014
[7] Zwick D and Muskulus M 2016 *Wind Energy* **19** 265–278
[8] Lin M and Porté-Agel F 2020 *Journal of Physics: Conference Series* vol 1618 (IOP Publishing) p 042036
[9] Saenz-Aguirre A, Ulazia A, Ibarra-Berastegi G and Saenz J 2022 *Energy Conversion and Management* **271** 116303
[10] Dowling N E 1971 Fatigue failure predictions for complicated stress-strain histories Tech. rep. Illinois Univ at Urbana Dept of Theoretical and Applied Mechanics
[11] Patel K and Freathy P 1984 *Engineering Structures* **6** 268–273

[12] Murtagh P, Ghosh A, Basu B and Broderick B 2008 *Wind Energy: An International Journal for Progress and Applications in Wind Power Conversion Technology* **11** 305–317
[13] Lackner M A and Rotea M A 2011 *Wind energy* **14** 373–388
[14] Si Y, Karimi H R and Gao H 2013 *Journal of Applied Mathematics* **2013**
[15] Stewart G M and Lackner M A 2014 *Engineering Structures* **73** 54–61
[16] Martin del Campo J O, Pozos-Estrada A and Pozos-Estrada O 2021 *Wind Energy* **24** 737–753
[17] Fitzgerald B and Basu B 2020 *Int. J. Sustain. Mater. Struct. Syst* **4** 347–372
[18] Lackner M A and Rotea M A 2011 *Mechatronics* **21** 704–719
[19] Fitzgerald B, Basu B and Nielsen S R 2013 *Structural Control and Health Monitoring* **20** 1377–1396
[20] Fitzgerald B, Sarkar S and Staino A 2018 *Journal of Sound and Vibration* **419** 103–122
[21] Arrigan J, Pakrashi V, Basu B and Nagarajaiah S 2011 *Structural Control and Health Monitoring* **18** 840–851
[22] Sarkar S and Chakraborty A 2018 *Structural Control and Health Monitoring* **25** e2083
[23] Smith M C 2002 *IEEE Transactions on automatic control* **47** 1648–1662
[24] Hu Y and Chen M Z 2017 *2017 29th Chinese Control And Decision Conference (CCDC)* (IEEE) pp 3056–3061
[25] Zhang R, Zhao Z and Dai K 2019 *Engineering Structures* **180** 29–39
[26] Sarkar S and Fitzgerald B 2020 *Structural Control and Health Monitoring* **27** e2471
[27] Sarkar S and Fitzgerald B 2022 *Engineering Structures* **266** 114558
[28] Jonkman J, Butterfield S, Musial W and Scott G 2009 Definition of a 5-mw reference wind turbine for offshore system development Tech. rep. National Renewable Energy Lab.(NREL), Golden, CO (United States)
[29] Jonkman J M 2010 *Definition of the Floating System for Phase IV of OC3*
[30] Kane T R and Levinson D A 1985 *Dynamics, theory and applications* (McGraw Hill)
[31] Hall M 2015 *Orono, ME: Department of Mechanical Engineering, University of Maine*
[32] Jonkman J and Buhl Jr M 2005 *National Renewable Energy Laboratory, Golden, CO, Technical Report No. NREL/EL-500-38230*
[33] Sarkar S, Chen L, Fitzgerald B and Basu B 2020 *Journal of Sound and Vibration* 115170
[34] Sarkar S and Fitzgerald B 2021 *Energies* **14** 6635
[35] MATLAB 2018 *version 9.4.0 (R2018a)* (Natick, Massachusetts: The MathWorks Inc.)
[36] Luft R 1979 *Journal of the Structure Division, ASCE* **105** 2766 – 2772
[37] Commission I E Iec 61400-3-1, wind turbines-part 3-1: Design requirements for offshore wind turbines, committee draft. sl: Iec, 2014 Tech. rep. IEC 61400-3-1
[38] Jonkman B J 2009 Turbsim user's guide: Version 1.50 Tech. rep. National Renewable Energy Lab.(NREL), Golden, CO (United States)
[39] Pierson Jr W J and Moskowitz L 1964 *Journal of geophysical research* **69** 5181–5190
[40] Hayman G and Buhl Jr M 2012 *National Renewable Energy Laboratory, Golden, CO* **74** 112